Excitation of N_2 in dc electrical discharges at very high E/n

B. M. Jelenković* and A. V. Phelps†

Joint Institute for Laboratory Astrophysics, University of Colorado and National Bureau of Standards, Boulder, Colorado 80309-0440

Spatial distributions of light emission from electric discharges in N_2 have been measured at very high electric-field-to-gas-density ratios E/n and low gas densities. The E/n range was from 270 Td to 107 kTd at gas densities from 1.3×10^{23} to 1.5×10^{21} m^{-3} (1 Td$\equiv 10^{-21}$ V m^2). Planar electrodes and low discharge currents, less than 3×10^{-4} A/m^2, insured that the electric field was spatially uniform. At the lower E/n and near the anode the intensities of first negative (1^-) and first (1^+) and second (2^+) positive bands of N_2 increased exponentially with distance as expected from published measurements of the spatial growth of ionization. The first and second positive band intensities were placed on an absolute scale by normalization to previously measured or calculated excitation coefficients for E/n of 270 to 700 Td. Because of the relatively weak signal at low E/n, the intensities of the first negative band at 391.4 nm are normalized to a theoretical value at extremely high E/n. At E/n above 4 to 30 kTd, depending on the transition observed, the emission peaked near the cathode. The N_2 first negative band emission near 391.4 nm can be largely accounted for by direct electron excitation of the $v=0$ levels of $B^2\Sigma_u^+$ state. Emission data from higher vibrational levels of the $B^2\Sigma_u^+$ state at very high E/n are consistent with excitation of N_2 by N_2^+. The first and second positive band emissions appear to be the result of electron excitation only at the lower E/n and at positions near the anode. The emission of these bands near the cathode at the higher E/n is postulated to be the result of excitation of the N_2 by about 100 eV molecules produced in charge-exchange collisions involving N_2^+ ions moving toward the cathode. The required excitation cross sections are approximately 10^{-20} m^2 for the $B^3\Pi_g$ group of states and 10^{-21} m^2 for the $C^3\Pi_u$ $(v=0)$ state.

I. INTRODUCTION

The initial and a continuing objective of this research is to test experimentally theories of the behavior of electrons at very high ratios of the electric field to gas density, E/n. The technique chosen was to measure the spatial dependence of the spectral emission from a low gas density, high voltage discharge and to compare measured and calculated electron induced emission rates. The relevant energy levels[1] of N_2, N_2^+, and N and the principal radiative transitions observed in this experiment are shown in Fig. 1. Since sources of excitation other than direct electron excitation appear to be present, we have the second objective of determining these sources of excitation and including them in models of the experiment. We have been successful in meeting the first objective for electron excitation of the first negative emission from N_2^+, but are able to provide quantitative models for other N_2 bands only at the lower E/n and near the anode.

Comparisons of experiment and theory under conditions in which electron excitation is dominant can be used to test calculation procedures[2-14] and cross sections[4,9,13,15] used to model the behavior of electrons in weakly ionized gases at very high E/n and at energies in the 10 eV to 10 keV range. Because of the uniform electric field in our experiment, the theory is simple enough to make definitive predictions. The results are expected to provide guidance for techniques being developed to

predict the behavior of nonequilibrium electrons and ions in such diverse phenomena as the cathode fall,[16,17] low pressure rf discharges for plasma processing,[18] the propagation of high frequencies through the ionosphere,[2,19] high-voltage discharges for switching,[20] charged-particle-beam propagation,[21] Tokamak start-up,[22] and high-field regions of semiconductors.[23]
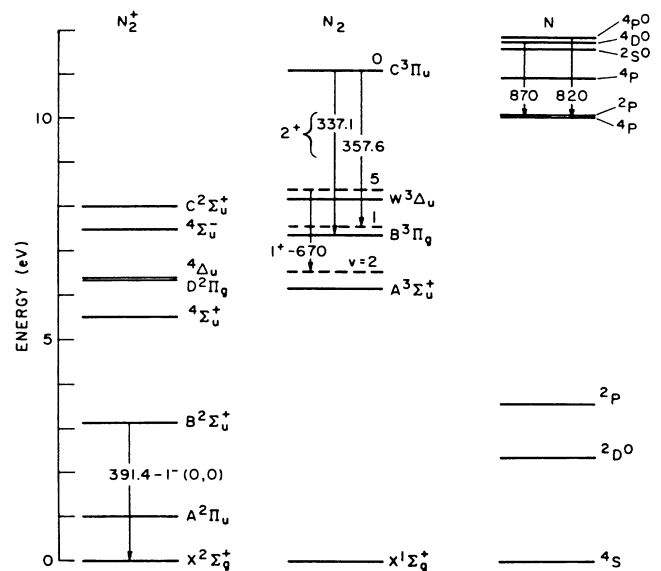

FIG. 1. Energy levels and radiative transitions relevant to this experiment.

The only previous experimental test of models of nonequilibrium electrons in spatially uniform electric fields at very high E/n was a measurement by Müller and Whale[24] of the energy distribution of electrons passing through low-density H_2 and was limited to maximum energies of 600 eV. These experiments showed evidence of beamlike behavior at sufficiently high E/n as predicted by the accompanying fluid model,[4] by other analytic models[2,3,5,8,9,22] and by Monte Carlo simulations for other gases.[6,10]

Experimental[6,25,26] and theoretical[5,6,11] investigations of electrical breakdown and low current, steady-state discharges at low values nd, where d is the electrode separation, are directly applicable to this problem. This previous work has demonstrated the importance of processes such as ionization by electrons backscattered from the anode, nonequilibrium or runaway behavior of the electrons, and the production of secondary electrons by ion and neutral bombardment of the cathode. Also of considerable relevance are previous theoretical and experimental studies of the ionization coefficients appropriate to the exponential temporal growth calculated to occur at very high E/n in magnetic fusion devices,[3,22] pulsed breakdown,[27] and radio-frequency breakdown.[28] Electron nonequilibrium phenomena in gases have been observed in which low-energy electrons emitted from a cathode undergo a delay in their ability to cause ionization[16] followed by quasiperiodic changes in the probability of ionization and excitation.[16,29]

The experimental apparatus and representative data are discussed in Secs. II and III. Section IV contains the theoretical relations used to convert the measured relative intensities to excitation coefficients. The experimental results are compared with theoretical predictions in Sec. V. The results of the work to date and future directions are summarized in Sec. VI. The Appendix presents a summary of the role of backscattered electrons in our experiments. The theoretical model used to calculate electron excitation and ionization coefficients from cross sections is given in the accompanying paper,[30] which will be referred to as II. Detailed models of excitation in ion-neutral and neutral-neutral collisions are still under development.

II. EXPERIMENT

The electron drift tube is shown in Fig. 2 and a schematic of the experiment is shown in Fig. 3. The electrodes are designed to provide a nearly spatially uniform electric field. A very important feature of the drift tube is the very uniform and closely fitting 80-mm-diameter quartz tube which prevents long path breakdown.[6,16,25,31] The drift tube is operated in the self-maintained discharge mode, for which previous measurements[25] and our measurements show that the discharge voltage is very nearly independent of current at low current densities, i.e., $<3\times10^{-4}$ A/m^2. This result is consistent with our prediction of small space-charge distortion of the electric field and of the absence of electron excited-state collisions. Although the operating voltage at low currents appears to equal the minimum breakdown voltage, at the higher E/n it is generally necessary
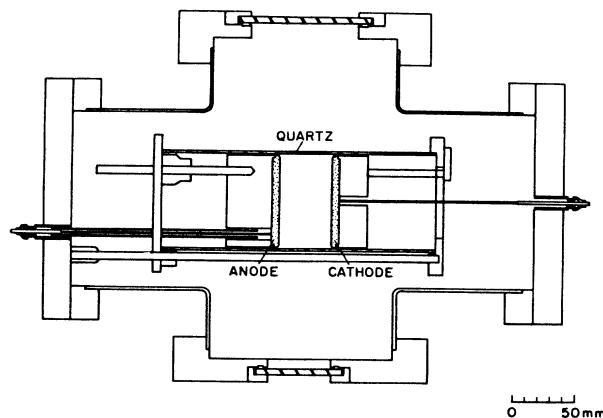

FIG. 2. Electron drift tube for high E/n experiment.

to initially apply a significantly larger voltage in order to obtain breakdown in a reasonable length of time.

The discharge electrodes are 78 mm in diameter and are made from either sintered graphite or 304 stainless steel. Except where noted, the anode was graphite and the cathode was stainless steel. The choice of carbon as an electrode material was based in part on the measured low yields of backscattered and secondary electrons[32] and desorbed ions[33] at the anode and in part on our trials of graphite, molybdenum, aluminum, and stainless-steel electrodes. We find that the discharge voltages are significantly higher with this graphite than with other materials tried. Figure 4 shows the measured operating voltage as a function of nd using various electrode combinations. The voltage-current characteristics are reproducible to about 1% once the discharge has been operated several hours. Discharge current oscillations observed at high E/n can be reduced from nearly 100% to less than about 5% by using a large resistor (10 to 100 MΩ) to control the average current and by connecting a moderate-size (0.5–5 nF) capacitor across the discharge. Because of difficulties in starting the discharge at the higher E/n and in order to discriminate against background light, a vacuum tube was connected in parallel with the discharge and was used to square-wave modulate the discharge current by 10–90 % at frequencies of
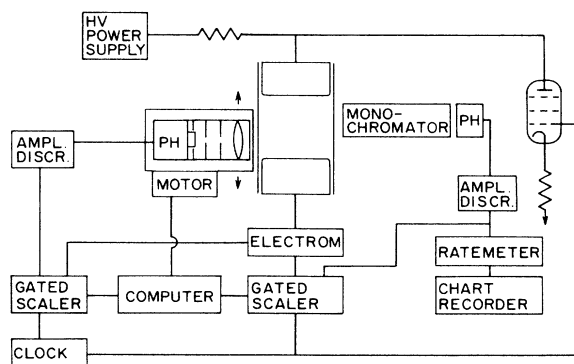

FIG. 3. Schematic of experiment for measurement of spatial distribution of light output at high E/n.
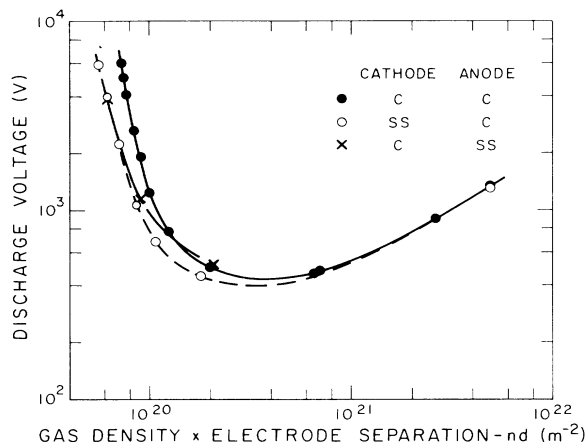
FIG. 4. Discharge operating voltage vs product of nitrogen density and electrode separation for sintered carbon (C) and stainless steel (SS) electrodes. These are also the minimum breakdown voltages.

a few Hz.

We have been able to operate the discharge at up to 6000 V without breakdown outside the main gap. The maximum E/n was approximately 100 kTd. (1 $Td \equiv 10^{-21}$ V m^2.) In these experiments the electrode spacing was either 36.1 or 38.6 mm. Visually the discharge appeared radially uniform, but deposits (cracked pump oil?) on the graphite cathode after several months operation suggest that the typical discharge diameter was 70 mm.

The light emission versus axial position data are obtained by mounting a photomultiplier and slit system on a table driven by a computer-controlled stepping motor. The position of this table was resettable by computer to about 0.1 mm in either direction of scanning. The emission was focused into a double-slit system[34] using a 70-mm-diameter quartz acromat lens. The initial adjustment of the slits gave a spatial resolution of about 1.5 mm [full width at half maximum (FWHM)], but was subject to significant shadowing by the electrodes and window flanges. Later "high-resolution" data were obtained with the slits set for about 1 mm resolution and much less shadowing near the electrodes. The resultant signal was reduced by a factor of about 40. Interference filters were used to select the wavelengths observed. The photomultiplier had a GaAs(Cs) photocathode with a nearly constant radiant sensitivity from 250 to 820 nm. The photomultiplier output passed through a counting chain and was stored in the computer. Typical integration times at a given position were 5 s and each reading was normalized to the current. Each curve shown is the average of several forward and backward scans.

The vacuum system is all stainless steel and copper with copper gasket seals except for the quartz windows which use indium gaskets. After a bakeout at 100 °C the pressure is less than or equal to 10^{-4} Pa with a rate of rise of less than or equal to 10^{-2} Pa/min. Since the gas samples are listed by the manufacturer to have 10^{-5} or less fractional impurities, the principal source of impurities was the background gas. The pressure was measured to $\pm 4 \times 10^{-2}$ Pa with a diaphragm manometer.

Voltage and current were measured with instruments stated to be accurate to $\pm 2\%$.

Emission spectra in the wavelength range from 250 to 890 nm were obtained with a $\frac{1}{4}$-m monochromator and GaAs(Cs) photomultiplier. The monochromator was set for 1–4-nm spectral resolution (FWHM) and had a field of view at the discharge of about 10 mm. Most of the spectral data were obtained from the region near the cathode because the signals at high E/n were larger there. The relative spectral sensitivity of the monochromator and detector in the 300–430-nm range was determined approximately using the branching ratios[1] for various transitions of the second positive system.

III. RESULTS

In this section we present the results of our measurements of the spectra and of the spatially dependent emission for the more prominent bands of N_2. Since no direct calibration of the sensitivity of the photomultiplier-detection system was made, our experimental data for each band are relative values as a function of position and E/n. The normalization of these data to obtain absolute excitation coefficients is discussed in Secs. IV and V. Brief summaries of these results which have been presented earlier[35] are superseded by those of the present paper.

A. Spectra

The spectral scans of the N_2 discharges were dominated by the first negative (1^-), first positive (1^+), and second positive (2^+) bands. The Meinel band system of N_2 was very weak because of severe quenching and the Vegard-Kaplan band system was not detected, probably because of destruction at the tube walls. The atomic N lines at 870 and 820 nm were particularly strong at the higher E/n. Lines of N I at 746 and 648 nm were also observed. The first three lines are emitted by the $2p^2(^3P)3p$ levels and the last radiates to these levels. These spectra and the data reported in this paper were obtained after running the discharge for several hours and changing gas several times, so that no impurity spectra were observed. Figure 5 shows representative spectra for 305–445 nm at E/n values of 290 Td and 78 kTd. The "stick spectra" of Fig. 5 were calculated using excitation coefficients for the $C^3\Pi_u$ and $B^2\Sigma_u^+$ states from Boltzmann calculations[15,36] at 290 Td, relative excitation coefficients for various vibrational levels based on electron beam[37] and swarm[38] experiments and recent radiative transition probabilities.[1,39] These predictions are in reasonable agreement with the experimental spectra. The spectra at very high E/n, such as that shown in Fig. 5 for 78 kTd, were more difficult to model. The stick spectra shown for the 1^- bands (dashed lines) at 78 kTd were obtained by increasing the populations of the higher vibrational levels relative to those found in electron beam experiments, e.g., by factors of 4 and 20 for $v = 1$ and 2, respectively. Such distributions of vibrational levels have been observed when N_2 is excited by moderate energy atomic[40] or molecular[41] ions. On the other hand, the second positive bands are much more in-
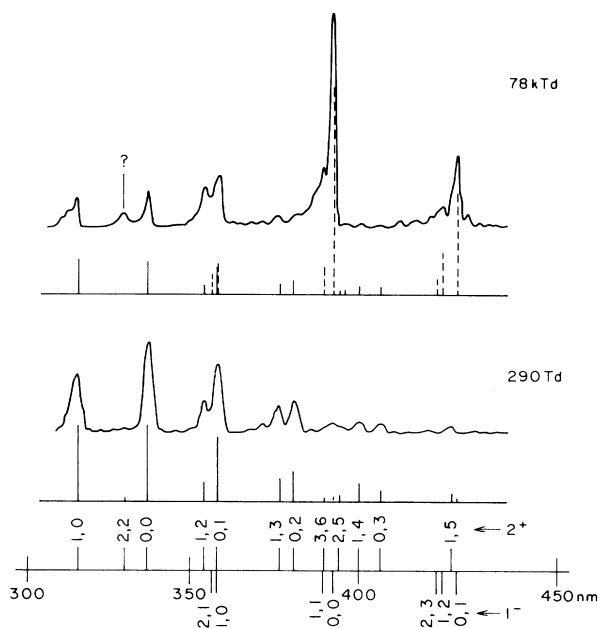
FIG. 5. Spectral scans of the 1$^-$ and 2$^+$ emission at representative E/n values. These data are not corrected for variations in monochromator transmission, etc. The dashed and solid lines for the 1$^-$ and 2$^+$ band systems shown immediately below the scans are calculated band intensities multiplied by the estimated relative detection efficiencies.

tense than expected from the published experimental ion-excitation data. More discussion of the intensities will be given in Sec. V.

B. Spatial scans

The points of Fig. 6 show values of the ratio of the measured photon-count rate to the discharge current as a function of position from cathode to anode for the first negative emission near 391±5 nm, i.e., the 0-0 band of the $B\,^2\Sigma_u^+$ to $X\,^2\Sigma_g^+$ transition. The apparent signals from positions far to the left of the cathode and far to the right of the anode are believed to be caused by scattered light reaching the detector. Data are shown for E/n values from 270 Td to 107 kTd. Our highest E/n is a factor of 30 higher than in previous light-emission[42] and current growth[43] experiments in N$_2$. From measurements for 0.6–6μA at E/n from 0.3–60 kTd we found that the emission signals for all bands scale directly with the discharge current as expected when space-charge effects and collisions between electrons and excited states or between two excited states are negligible. The first negative emission is of particular interest because its excitation cross section has a maximum at the same energy as that for the total ionization cross section, so that this signal is a measure of the presence of electrons which can cause ionization.

The points of Fig. 7 show measured count rates versus position normalized to the discharge current for an interference filter transmitting 337±5 nm (FWHM), i.e., from the 0-0 band of the $C\,^3\Pi_u$ to $B\,^3\Pi_g$ transition. At $E/n =270$ Td the spatial dependences of the 391.4 and
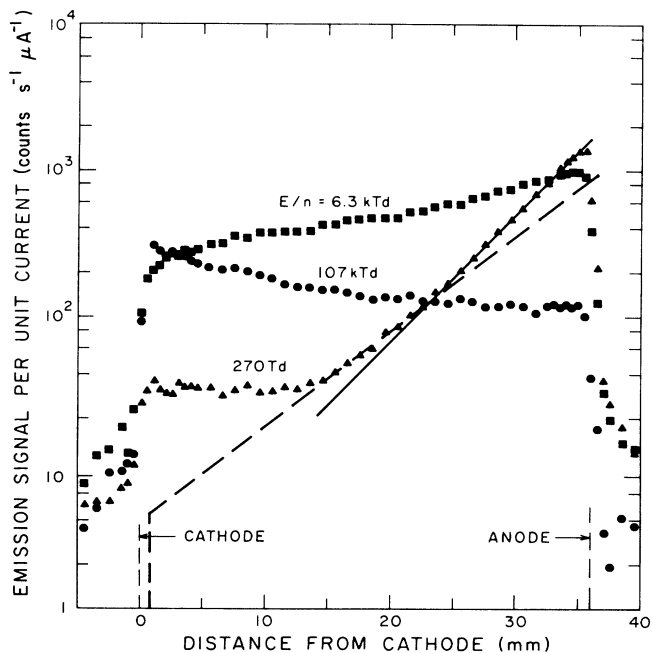

FIG. 6. Spatial dependence of 391.4-nm (1$^-$) band emission from N$_2$ discharges at various E/n. The symbols, E/n in Td, and gas densities in m^{-3} used are ▲, 270, 1.35×10^{23}; ■, 6300, 3.0×10^{21}; ●, 108,000, 1.545×10^{21}. Only alternate experimental points are shown except near the electrode positions. The solid line shows our interpretation of the 270-Td data in terms of an exponential growth of electron density, while the dashed lines show the variation of emission expected from the ionization growth parameters of Ref. 43.
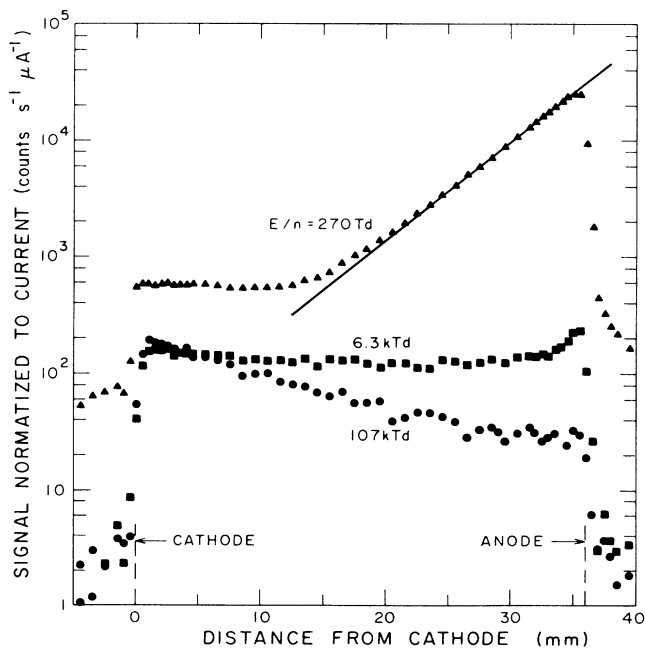

FIG. 7. Spatial dependence of 337.1-nm (2$^+$) band emission from N$_2$ discharges at various E/n. The gas densities used were the same as for Fig. 6. The points and solid line are as in Fig. 6.

337.1 bands agree to within the statistical fluctuations, but for $E/n > 1000$ Td significant differences develop. This higher E/n data will be discussed in Sec. V. Note the peak in the 337.1-nm emission near the anode for $E/n = 6.3$ kTd. We believe that this effect is caused by backscattered electrons and will discuss such data in the Appendix.

The points of Fig. 8 show measured values of the count rate normalized to the discharge current for the 670-nm band of N_2, i.e., from the 5-2 band of the $B\,^3\Pi_g$ to $A\,^3\Sigma_u^+$ transition as a function of position. Note that these data were obtained with our "low-resolution" optics and so have much higher count rates and less scatter than the data of Figs. 6 and 7. Comparison of data obtained using both optical systems at 391.4 nm and a common E/n indicates that the low-resolution data obtained closer than 4.5 mm from the cathode and 2 mm from the anode are reduced in magnitude by 10% or more as the result of shadowing by the electrodes and by the window mount. We therefore restrict our discussion of the data of Fig. 8 and succeeding figures to the regions between the vertical bars.

Data such as those of Figs. 6–8 show that at E/n below about 10 kTd for the 1^- emission and below 1 kTd for the 1^+ and 2^+ emission the signal increases exponentially with distance as one approaches the anode. As has been done by others,[42] we have interpreted this dependence as evidence of an exponential growth of electron density resulting from an electron avalanche. The points of Fig. 9 show the spatial ionization coefficients
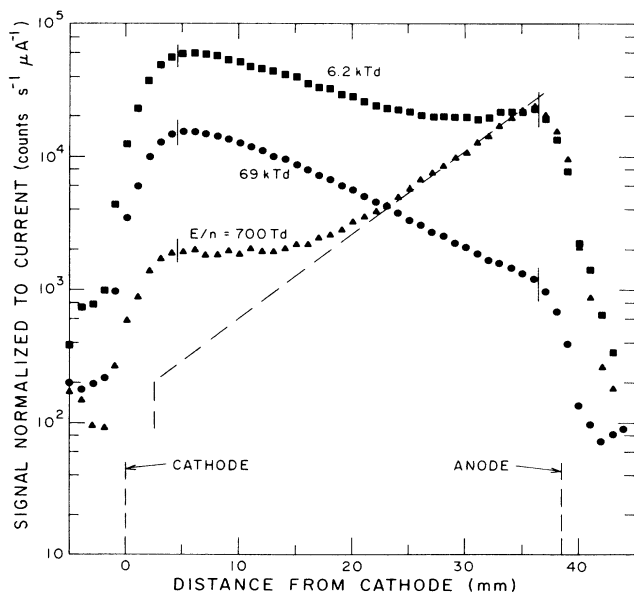

FIG. 9. Spatial ionization coefficients vs E/n for electrons in N_2. The points are obtained from fits to our experiments such as shown by the solid straight lines of Figs. 5 and 7. The circles and crosses are for carbon and stainless-steel anodes, respectively. The solid curve is from the current growth data of Ref. 43. The dashed curve is calculated using the single-beam, energy-balance model presented in paper II.

obtained from fits to the data, such as shown by the solid straight lines of Figs. 6–8. The solid circles and crosses show results obtained with the graphite and stainless steel anodes, respectively. The results of published measurements[43] of the spatial-ionization coefficient[44] for electrons in N_2 are shown by the solid curve. The dashed curve of Fig. 9 shows the results of calculations using the single-electron-beam model discussed in II.

IV. THEORY OF EXPERIMENT

In this section we wish to present the models used for comparison of our experimental spatial-emission profiles with the predictions of theory. We will first review the collision processes which are potentially important in the production of the observed emission. We will then discuss the determination of relative and apparent excitation coefficients and their normalization to experimental data or theory.

A. Excitation processes

The first excitation process considered is direct electron excitation of N_2. We will use a recently proposed[15] set of electron-collision cross sections to calculate electron distribution functions and spatial ionization and excitation coefficients.[44] In Sec. V we will consider the magnitude of the production by high-energy electrons of excited ions, atoms, and molecules which then may produce excited molecules in low-energy excitation-transfer collisions with N_2.

The excitation of molecules and atoms by ions and the associated fast atoms and molecules produced in ion-

FIG. 8. Spatial dependence of 670-nm (1^+) band emission from N_2 discharges at various E/n. The symbols, E/n in Td, and gas densities in m^{-3} are ▲, 700, 1.68×10^{22}; ■, 6200, 3.2×10^{21}; ●, 69,000, 1.9×10^{21}. The short vertical lines associated with each set of points show the estimated limits of reliable data as obtained with the "low-resolution" optics. The dashed line shows that our exponential fit to these data agrees well with that predicted from Ref. 43.
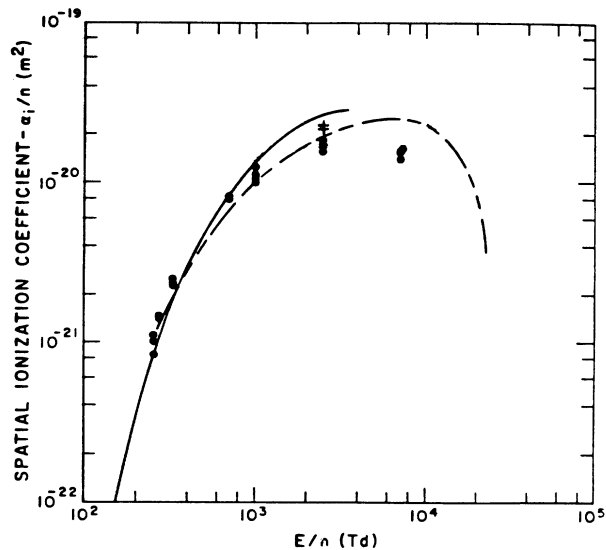
molecule collisions at very high E/n is an almost completely unexplored field. The only related data appear to be those in which the 2^+ emission was used to monitor the behavior of fast $N_2(X\,{}^1\Sigma_g^+)$ and $N_2(A\,{}^3\Sigma_u^+)$ beams[45] and those for excitation of the 1^- and 1^+ bands in high-temperature shock waves[46] in collisions of N and N_2. Although ion avalanches have been found important in models of breakdown[5,6,11] at low nd and very high E/n, there appears to be no direct experimental determination of the growth coefficients for ion avalanches in N_2.[16] Significant ion avalanching in our experiment would produce an exponential growth toward the cathode of any ion or fast neutral induced emission in a manner similar to the exponential growth toward the anode for electron-induced excitation in an electron avalanche. Recent observations[47] of Doppler-shifted and broadened spectra from regions of high electric fields present in the cathode fall of low pressure, moderate current discharges have pointed to the importance of excitation by fast ions or atoms.

The third group of excitation processes of potential importance here begins with the reflection of fast ions as neutralized and excited fast atoms or molecules on impact with the cathode. This process has been observed using ion beams in vacuum.[48,49] Excited-state production at surfaces has been inferred from the Doppler shift and broadening observed in the cathode fall of discharges.[47,50] The only quantitative observations[49] of emission by excited states of the neutralized incident ion appear to be for atomic H. The fast excited atoms formed by this process may radiate or may collisionally excite the gas molecules to the observed levels. We have not found any beam measurements of the reflection of N^+ or N_2^+ as excited atoms or molecules. This process is considered quantitatively in Secs. IV D and V D.

B. Experimental excitation coefficients

Since the procedures for the determination of excitation coefficients in drift tubes have been discussed in detail by Lawton and Phelps,[51] we make use of the relationships developed by these authors for the signal produced by the photomultiplier system. In particular, the excited-state density n_k for neutral molecules is found by solving the continuity equation in one-dimensional geometry, i.e.,

$$V_z \frac{dn_k(z)}{dz} = -An_k(z) - k_q nn_k(z)$$

$$+ n_e(z)n \int_0^\infty vQ_e^k(v)f_e(v,\theta,z)d^3v \;, \quad (1)$$

where V_z is the z component of velocity of the excited molecules, A is the total radiative transition probability, k_q is the rate coefficient for collisional quenching of the excited state, n_e is the density of the electrons, v is the relative speed of the electron and the ground-state molecule, n is the ground-state density, Q_e^k is the cross section for excitation of the molecules by electrons, θ is the angle the electron velocity makes with its direction of acceleration due to the electric field, and $f_e(v,z,\theta)$ is the

spatially dependent velocity distribution for the electrons. If excitation by ions or neutrals is important Eq. (1) will contain additional terms, which will be similar to the last term. In this case the velocity of the excited species may be very high. Since the emission data of Sec. III vary slowly with distance we neglect the derivative term in Eq. (1). The validity of this assumption will need to be examined more closely once the major excitation processes are determined.

We eliminate n_e using the definition of the electron-current density given by

$$j_e(z) = en_e(z)\int_0^\infty v\cos\theta f_e(v,\theta,z)d^3v \;. \quad (2)$$

The spatial excitation coefficient per unit distance in the direction of flow of charge normalized to the gas density $\alpha^k(z)/n$ is defined as the ratio of the rate coefficient for excitation, i.e., the integral in Eq. (1), to the convective drift velocity, i.e., the integral in Eq. (2). From Eqs. (1) and (2) $\alpha_i(z)/n$ is found to be

$$\frac{\alpha^k(z)}{n} = \frac{\int_0^\infty vQ_e^k(v)f_e(v,\theta,z)d^3v}{\int_0^\infty v\cos\theta f_e(v,\theta,z)d^3v}$$

$$= \frac{n_k A}{n} \frac{e}{j_e} \frac{(A+nk_q)}{A} \;. \quad (3)$$

Here $n_k A$ is the rate of photon emission per unit volume and is normalized to the electron flux j_e/e and to the gas density. In the limit of low E/n, where the electron-velocity distributions are independent of position, this spatial-excitation coefficient is independent of position and is a function only of E/n. In the limit of extremely high E/n, the electrons undergo free-fall motion from the cathode and all have the same velocity. If the quenching is small, then this excitation coefficient reduces to the excitation cross section and is a function only of the electron energy as given by $\epsilon(z) = e(E/n)(nz)$. In Eq. (3) the fraction of the excited states which radiate before being quenched $A/(A+nk_q)$ can be written as $(1+n/n_0)^{-1}$, where $n_0 = A/k_q$ is a "quenching density."

The steady-state signal $S(z)$ measured when the detector is focused at a position z relative to the cathode is[51]

$$S_k[z] = f_w AD(v_i)\langle f_i\rangle(\Delta\Omega/4\pi)\int_V \eta n_k \, dv$$

$$= f_w D(v_i)\langle f_i\rangle(\Delta\Omega/4\pi)\langle\eta\rangle V$$

$$\times \frac{n}{(1+n/n_0)} \frac{j_e(z)}{e} \frac{\alpha_k(z)}{n} \;, \quad (4)$$

where

$$\langle f_i\rangle = \int_0^\infty f_i(v)R_k(v)dv \Big/ \int_0^\infty R_k(v)dv \;. \quad (5)$$

Here f_w is the fractional transmission of the lens, slits, windows, and quartz tubing between the excited molecules or atoms and the photomultiplier; $D(v_i)$ is the efficiency per photon of the photomultiplier and counting chain at the frequency of peak transmission of the interference filter; $f_i(v)$ is the fractional transmission of

the interference filter at the frequency v; $\langle f_i \rangle$ is the fraction of the radiation emitted by the excited electronic state which is transmitted by the interference filter; $R_k(v)$ is the relative intensity of radiation emitted by the atoms or molecules in the electronic state in the frequency interval dv; $\Delta\Omega$ is the effective solid angle subtended by the detection system from the axis of the drift tube; and η is the efficiency of the photon collection versus position in the tube for a fixed position of the movable photomultiplier table. Here we have assumed that the transmission of the windows, the sensitivity of the detector, etc., vary slowly with frequency compared to $f_i(v)$. Mappings of the light collection efficiency with a miniature light-emitting diode and dummy metal electrodes mounted as in the drift tube showed that the spatial resolution with the high-resolution optics was 1 mm FWHM for all positions of the table and varied by less than 50% for the extreme radial positions in the drift tube. The collection efficiency for points on axis of the discharge tube and for various table positions was found to be constant in magnitude to within 10% for distance greater than 3 mm from the electrodes. We therefore assume that the integral in the first form of Eq. (4) can be replaced by an average collection efficiency $\langle \eta \rangle$ times a fixed volume times the excited atom density to obtain the second form of Eq. (4). This will lead to error in the spatial scans near electrodes.

The evaluation of $\langle f_i \rangle$ is somewhat involved in the present experiments because of the wide range of relative intensities encountered and, in unfavorable circumstances, the resultant transmission by the filters of significant intensities from bands other than the desired band. For example, transmission of the $2^+(2,5)$ band at 394.3 nm through the interference filter used for the $1^-(0,0)$ band at 391.4 nm severely limited the accuracy of the 1^- data at low E/n. Similarly, interference by the $1^-(1,0)$ band near 358.2 nm led to large and somewhat uncertain corrections to the data for the $2^+(0,1)$ band near 357.6 nm at high E/n. The data for the $2^+(0,0)$ band near 337.1 nm and the $1^+(5,2)$ band near 670 nm appeared to be free of significant interference.

Thus far the results of calculations have been presented in terms of the number of excitation events at a point z per unit distance in the direction of acceleration $\alpha^k(z)$. This excitation coefficient is essentially the rate of excitation by electrons normalized to the local electron current density or alternatively the ratio of the local rate coefficient for excitation to the local convective velocity. In order to relate these calculations to the measured total discharge current we define an "apparent" excitation coefficient $\beta^k(z)$ given by

$$\beta^k(z) \equiv \frac{j_e(z)}{j_T}\alpha^k(z) = \frac{j_e(z)}{j_e(d)}\alpha^k(z) \ . \tag{6}$$

In writing the second form of Eq. (6) we have made the assumption that the yield of desorbed ions resulting from electron bombardment of the anode is negligible so that the electron current density at the anode equals the total discharge current density, i.e., $j_e(d)=j_T$. In Sec. V and in the Appendix the experimental apparent excitation

coefficients normalized to the gas density will be compared to the theoretical results from II. Note that although Eqs. (3) and (6) were derived with electron excitation in mind, they are readily extended to include excitation by fast ions or fast neutrals.

C. Normalization of data

In view of the good agreement shown in Fig. 9 between the observed exponential spatial growth of emission and the growth expected from previous measurements and calculations of the spatial ionization coefficient, we will use electron-excitation coefficients measured previously[36,38,52] for the $C\,^3\Pi_u$ state and calculated[15] for the $B\,^3\Pi_g$ group of states of N_2 to convert the relative emission intensities to absolute excitation coefficients. Because of the large uncertainties in the 391.4-nm data at the lower E/n, these data will be normalized to the theory of II at high E/n.

The absolute excitation coefficients derived from the observed 1^+ and 2^+ band emission at the anode are shown by the squares and circles of Fig. 10, respectively, for the entire range of E/n. The data points are obtained by normalizing the observed count rates per unit current at the anode to the smooth curves at E/n between 250 and 700 Td. From Eqs. (4) and (5) the excitation coefficient at any E/n is related to the fitted excitation coefficient by

$$\frac{\beta^k}{n}[E/n,nd]$$
$$= \frac{S_k(E/n,nd)(1/n+1/n_0)}{S_k[(E/n)_r](1/n_r+1/n_0)}\frac{\langle f_i \rangle}{\langle f_i \rangle_r}\frac{\beta^k}{n_r}[(E/n)_r]\frac{n_r}{n}\ , \tag{7}$$

where the subscript r indicates values obtained at the low reference E/n and the unsubscripted parameters indicate values obtained at the higher E/n and nd.

The measured 1^+ and 2^+ intensities extrapolated to the position of the anode are used in the normalization since, in the absence of significant electron-induced desorption of ions,[33] the electron current at the anode is equal to the measured total current. This means that in the vicinity of the anode only electrons can cause excitation. In addition, we will assume that at these lower E/n the effects of electrons reflected by anode can be neglected. At the higher E/n we rely on the use of a graphite anode and the extrapolation to minimize the effects of backscattering. Note that in applying these calibrations to the higher-E/n data we make the assumption that the spectral distribution of the emission does not change significantly with E/n, i.e., that $\langle f_i \rangle$ in Eq. (5) is constant. See the following discussion of collisional quenching and mixing.

Because of the uncertainties at low E/n in the corrections for light leakage through the interference filter used for the 391.4-nm band and for quenching, we have normalized the 391.4-nm data to the predictions of the single-beam, energy-balance model of II at E/n values between 69 and 107 kTd. Furthermore, we have carried out the normalization at a point 20 mm from the
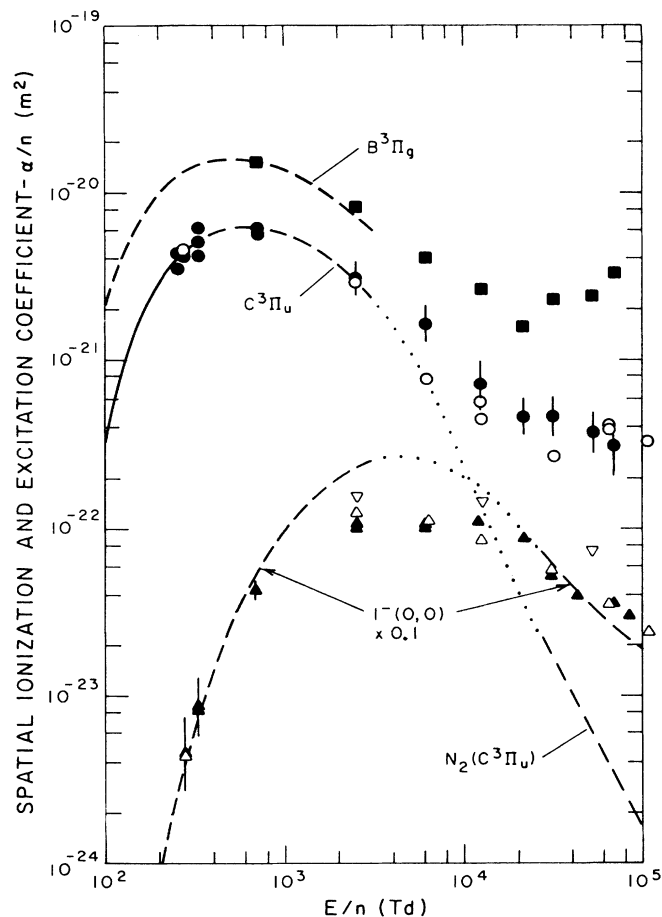
cathode rather than at the anode, so as to minimize the effects of backscattered electrons and electrode shadowing. As a result of fitting at midgap, the triangular points of Fig. 10 for the apparent excitation coefficient β/n at the anode are somewhat above the theory at the highest E/n.

A source of uncertainty in the normalization procedure is in the correction for collisional quenching of the important energy levels of Fig. 1. The values used for the densities n_0 at which 50% of the radiation is lost to quenching are listed in Table I. The quenching data for the $B\,^2\Sigma_u^+$ state[53,54] of $N_2{}^+$, and $C\,^3\Pi_u$ state,[54] and the $B\,^3\Pi_g$ state[55,56] of N_2 are badly scattered. Note that our $B\,^2\Sigma_u^+$ quenching rate coefficient is significantly lower than measured room-temperature values[53,54] since we have extrapolated the measured temperature dependence[57] to the ion energies expected at our lower E/n. These energies were calculated[58,59] from measurements of charge-exchange cross sections[60] for ground state $N_2{}^+$. The quenching density used for the $B\,^3\Pi_g$ state is consistent with values for the decay of the combined $B\,^3\Pi_g$ and $W\,^3\Delta_u$ states,[56] i.e., based on the observed intensity distributions of the 1^+ band in our experiments we have assumed that the B, W, and B' states are collisionally mixed at the N_2 densities of our experiments. The detailed effects of collisional mixing on the 1^+ spectra have been investigated[61] for upper atmospheric conditions. Analyses have been made[62] of the effects of a dc discharge at low E/n on the vibrational populations of the $C\,^3\Pi_u$ state. We were unable to detect changes in the relative intensities of the important bands of the 2^+ system.

FIG. 10. Spatial excitation coefficients vs E/n for various excited states of N_2. The points are obtained from our experiments. The open and closed points were obtained with different interference filters as discussed in the text. The dashed curves for $E/n < 3000$ Td are from the calculations of Ref. 15, while the dashed curves for higher E/n are from the single-beam model of paper II. The solid curve shows the average experimental results of Refs. 36, 38, and 52. The experimental excitation coefficients and the theoretical curves for $E/n > 10$ kTd are for conditions at the anode as discussed in the text. The dotted curves are rough estimates drawn to aid the eye in connecting calculations.

D. Excited species from cathode

A simple relation can be derived for the apparent excitation coefficient β_s^k for the production of excited atoms or molecules as the result of ion bombardment of the cathode. The flux of such excited species $n_k V_k$ leaving the cathode is given by

$$n_k V_k = \frac{j_+}{e} R_k = \frac{j_T}{e}\frac{R_k}{(1+\gamma_+)}\ ,\qquad(8)$$

where n_k and V_k are the density and the normal com-

TABLE I. Quenching data used in analysis of experiments.

Excited state	Radiative lifetime (s)	Quenching rate coefficient (m^3/s)	Quenching density $-n_0$ (m^{-3})
$N_2{}^+$ $B\,^2\Sigma_u^+(v=0)$	$6.2[-8]^{a,b}$	$1.6[-16]^c$	$1.0[23]$
N_2 $B\,^3\Pi_g(v=5)$	$6.2[-6]^d$	$7.3[-18]^d$	$2.2[22]$
N_2 $C\,^3\Pi_u(v=0)$	$3.7[-8]^a$	$1.3[-17]^e$	$2.2[24]$

[a]Reference 1.
[b]$6.2[-8]$ means 6.2×10^{-8}.
[c]See text for source of value.
[d]D. C. Cartwright, Ref. 56.
[e]Reference 54.

ponent of the velocity of the excited species, j_+ and j_T are the positive ion and measured total current densities, R_k is the yield of fast excited atoms or molecules per incident ion, and γ_+ is the yield of electrons per incident ion. In the limit of small quenching appropriate to our highest E/n data, the apparent excitation coefficient at $z=0$ is then given by

$$\beta_s^k(0)=\frac{eAn_k}{j_T}=\frac{AR_k}{(1+\gamma_+)V_k} \; . \tag{9}$$

Note that this excitation coefficient is principally dependent on the ion velocity, which determines R_k, γ_+, and V_k. We have no information on this dependence for nitrogen ions. β_s^k is independent of the gas density, although it is necessary to divide by the gas density in order to compare with the data presented in Figs. 10–13. If the excited species were produced by fast neutrals incident on the cathode, the right-hand side of Eq. (9) would be multiplied by the ratio of the neutral flux to the ion flux. This ratio could well depend on E/n and nd.

The density of excited species and the apparent excitation coefficient will decrease with distance from the cathode due to radiative decay and collisional quenching of the excited state. Neglecting collisions, as is approximately correct for the $B\,^2\Sigma_u^+$ and $C\,^3\Pi_u$ states, gives an upper limit to the apparent excitation coefficient of

$$\beta_s^k(z)=\beta_s^k(0)e^{-z/\lambda} \; , \tag{10}$$

where $\lambda=V_k/A$. If there were many scattering collisions during the lifetime of the emitted excited state, as expected for the $B\,^3\Pi_g$ group of states, the exponential dependence of the apparent excitation coefficient of Eq. (10) would be replaced by a linear decrease with distance as predicted by a solution of the diffusion equation. The magnitude would be much lower than in Eq. (10) because of the loss of excited molecules due to backscattering to the cathode.

V. COMPARISON OF THEORY AND EXPERIMENT

Figures 6–8 and 10–12 show comparisons of our experimental results with the results of previous low-E/n experiments where available and with predictions of the single-beam models for electrons derived in II for high E/n. In this section we will show that the agreement of the spatial dependence and magnitude of the predicted and measured emission is satisfactory at low E/n only for positions toward the anode and at high E/n only for the 391.4-nm emission from N_2^+ ions. We will suggest that the excess emission from the $B\,^3\Pi_g$ and $C\,^3\Pi_u$ states of N_2 near the cathode at high E/n is due to excitation of the N_2 by fast N_2 molecules produced in collisions of N_2^+ with N_2.

A. Spatial dependences at low E/n

The spatial ionization coefficients derived from the slope of semilogarithmic plots of intensity versus position near the anode at E/n below 1000 Td and shown by

the points of Fig. 9 are in reasonable agreement with the previous experimental data shown by the solid curve. At E/n above 1000 Td our data suggest spatial ionization coefficients which are significantly lower than the values derived from current growth experiments.[43] Our ionization coefficients are, however, more consistent with the more detailed electron-beam-type models as discussed in II.

The spatial dependences of the N_2 band emission at low E/n plotted in Figs. 6–8 show large departures from the simple exponential growth at positions near the cathode. Some departure close to the cathode is expected on the basis of the observed "nonequilibrium distance" required for the ionization rate to reach its equilibrium value.[10,16,29] From Monte Carlo calculations[63] one would expect that this equilibrium effect would result in a low intensity of the light output for a distance from the cathode corresponding to a voltage change equal to a few times the excitation potential. The light should then follow the increasing electron density. This prediction is shown schematically by the bold dashed lines of Fig. 6, where the exponential growth is based on measured ionization-growth data.[43] Experimentally one sees excess emission from near the cathode to about halfway across the gap. The data of Figs. 7 and 8 show a similar excess emission for the 337.1- and 670-nm bands. Excess emission near the cathode was observed previously by Blassberg and de Hoog[42] in H_2 for the Balmer-series emission. Although we have not made an extensive investigation, we have no viable hypothesis to explain the difference between the observation and the expectation for low E/n in N_2. For example, higher than average E/n values near the cathode due to ion space charge appear ruled out by the absence of changes in the spatial dependence of emission for an order of magnitude change in current at 330 Td. Emission resulting from excited atoms produced by the impact of ions with the cathode surface[48] seems very unlikely over these large distances at the low ion energies (~ 1 eV) and high gas densities of these measurements (see Secs. IV D and V D). More careful measurements, including additional tests for scattered light from the relatively intense emission near the anode, are needed. Clarification of the source of the excess emission near the cathode may help explain the differences in the spatial ionization coefficient from Haydon and Williams[43] (dashed line in Fig. 6) and the ionization coefficient derived by fitting our data near the anode (solid line).

B. E/n variation of excitation

Figure 10 shows the apparent excitation coefficients for the production of the $B\,^3\Pi_g$ and $C\,^3\Pi_u$ excited electronic states of N_2 as determined by normalizing the 1^+ and 2^+ band emission as described in Sec. IV C. An average of the published[36,38,52] experimental excitation coefficient data for the $C\,^3\Pi_u$ state is shown by the solid curve. The dashed curves at $E/n < 2$ kTd show the results of calculations using recently recommended cross sections and the two-term solution to the Boltzmann equation.[15] The dashed curve at $E/n > 10$ kTd was cal-

culated using the single-beam model of II and the relevant cross sections.[15] The excitation coefficients at the anode at the higher E/n depend on the nd product through $V=(E/n)(nd)$, i.e., the $1^-(0\text{-}0)$ coefficient is very nearly equal to the 391.4-nm excitation cross section at the discharge voltage used for the particular measurement. This is not the case at low E/n where the excitation coefficients are expected to be independent of position and nd beyond the short equilibration distance from the cathode.

Very little error due to changes in the spectral distribution is expected for the C-state excitation coefficients at high E/n since quenching effects are calculated to be less than 10% for all of our experiments. A source of uncertainty for the C-state data obtained using the 357.6-nm band and the low-resolution optics is the correction for 1^- band transmission through the interference filter at high E/n discussed in Sec. IV B. The corrected data with estimated uncertainties are shown by the solid circles with error bars in Fig. 10. Such uncertainties are not present in the later data obtained from the $337.1(2^+0,0)$ band using the high spatial resolution optics and shown by the open circles.

It should be kept in mind that the calculated excitation coefficient for the $B\ ^3\Pi_g$ state is actually the sum of the calculated values for the $B\ ^3\Pi_g, W^3\Delta_u, B'\ ^3\Sigma_u^-,$ $C\ ^3\Pi_u$, and $E\ ^3\Sigma_g^+$ states, where the latter two states are assumed to cascade to the $B\ ^3\Pi_g$ state. Since the N_2 densities of our experiment are well above those at which the major changes in the spectral distribution of the 1^+ band have been observed,[61] we expect and observe that the division of the emission from among the vibrational levels of the $B\ ^3\Pi_g$ state is independent of E/n and n.

Note that we have evaluated the excitation coefficient for the 391.4-nm $(1^-0,0)$ band rather than for the $B\ ^2\Sigma_u^+$ state. One reason for this is the large amount of excitation-cross-section data[15,64] for this band. A second reason is the changing vibrational populations inferred from the spectra in Fig. 5. The values of the excitation coefficients for the 391.4 band at low E/n derived from this fitting at high E/n and the use of Eq. (7) are compared with the values calculated using the Boltzmann equation[15] in Fig. 10. Because of the uncertain corrections ($\pm50\%$) at these low E/n, one must be cautious about regarding the apparent agreement between theory and experiment as a test of theory or of the quenching rate coefficient.

We see from Fig. 10 that the electron-excitation coefficients for the $N_2(C\ ^3\Pi_u)$ state calculated using Eq. (18) of II for the contribution of secondary electrons produced by ionization to the excitation are two orders of magnitude smaller than the values derived from the emission near the anode. Although not shown, a similar discrepancy is found for the excitation of the $N_2(B\ ^3\Pi_g)$ state. Note that for both the C and B states of N_2 there is a sharp break in the apparent excitation coefficients versus E/n near 20 kTd, suggesting a change in the excitation mechanism at the higher E/n. We will discuss the problem of explaining the excitation of the N_2 triplet states in Secs. V C and V D.

C. Spatial variation of excitation

Having established the absolute values of the excitation coefficients, we now compare the spatial variations of the apparent excitation coefficients with theory.

1. First negative band

The solid curves of Fig. 11 show the experimental spatially dependent excitation coefficients for the 391.4-nm band emission from the $v=0$ levels of the $N_2^+(B\ ^2\Sigma_u^+)$ state obtained at the higher E/n using the high-resolution optics. The dashed curves show the results of calculations of electron excitation[64] using the single-beam models of II. Note that the upper and lower pairs of curves have been shifted by factors of 10 to reduce overlapping. We consider the agreement to be very good in view of the approximate nature of the single-beam model for the electrons. The less-sharp peak in the experimental data near the cathode at $E/n=107$ kTd compared to the calculated curve may be the result of limitations of the detection system but is more likely caused by errors in the single-beam model with its monoenergetic electrons. The changing ratio of experiment to theory as the anode is approached at 107 kTd and the slight peak near the anode at 31 kTd is believed to be the result of backscattered electrons (see the Appendix). The general agreement of the variation in magnitudes with E/n is encouraging. It is of interest to note that the nearly flat theoretical curve for 31 kTd is the re-
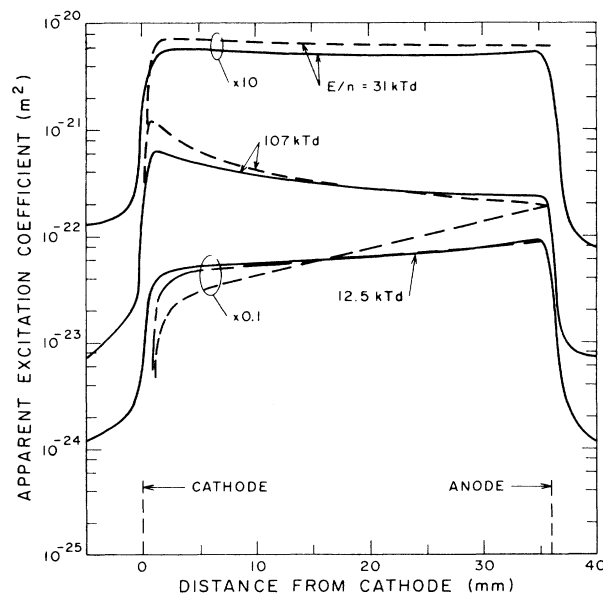

FIG. 11. Comparison of experimental apparent excitation coefficients (solid curves) for the 391.4-nm band of the N_2^+ $B\ ^2\Sigma_u^+\text{-}X\ ^2\Sigma_g^+$ transition with theoretical predictions (dashed curves). The solid curve for 107 kTd is drawn through the values shown in Fig. 6. The curves for 12.5 and 31 kTd are for N_2 densities of 2×10^{21} and 2.4×10^{21} m^{-3}, respectively. These data are normalized as discussed in the text. The chain curve is calculated using the single-beam, energy-balance model for electron motion and excitation derived in II. The dashed curves are for the single-beam, momentum-balance model.

sult of about a factor of 3 decrease in the excitation cross section which is balanced by a corresponding increase in electron current due to avalanche ionization. In the 107-kTd case, the ionization avalanche is insufficient to make up for the decrease in cross section, i.e., the electron multiplication across the gap is only 1.4. Note the slower rise in the calculated and experimental emission curves near the cathode for 12.5 kTd than calculated for the high E/n. This rise is caused by the increasing excitation cross section with increasing electron energy.

The two dashed curves shown for the 12.5-kTd case in Fig. 11 illustrate the differences between results obtained with the two single-beam models presented in II. The short dashed curves for all three cases in Fig. 11 are calculated using the single-beam, momentum-balance model, while the long-short dashed curve for 12.5 kTd is calculated using the single-beam, energy-balance model. In general, the energy-balance model yields higher apparent excitation coefficients at low nz and lower values at large nz than does the momentum-balance model. The energy-balance model is seen to be particularly useful at the lower E/n. For the highest E/n and our nd values the predictions of the two models are indistinguishable.

A complication in this rather satisfactory situation is the evidence of a significant contribution to the 1^- band system excitation by heavy particles provided by the appearance of relatively strong emission from vibrational excited states of the $B\,^2\Sigma_u^+$ state at E/n above 46 kTd. This effect is shown by spectra such as that of Fig. 5. Our very approximate estimates[58] of the excitation of the 391.4 band by ions using published data indicate that the excitation of the 391.4-nm band by N_2^+ is never more than about 10% of the observed value. On the other hand, this calculation of excitation by N_2^+ shows that the sum of the excitation coefficients for the higher vibrational levels is comparable with the observed values over a wide range of E/n. More accurate spectral-distribution data and models would be needed for a quantitative comparison.

2. First and second positive bands

In contrast to the rather good agreement between the electron-excitation model and experiment found for the $N_2^+(B\,^2\Sigma_u^+)$ state, the curves of Fig. 12 show that direct electron excitation is much too small to explain the observed excitation of the $C\,^3\Pi_u$ and $B\,^3\Pi_g$ states. The solid curves of Fig. 12 show the only available data for the three states at fixed E/n. The data were obtained using the low-resolution optics and are normalized to other low-resolution data as discussed in Sec. V B. Only the portions of solid curves between the vertical bars should be compared with theory. The middle dashed curve shows the calculated 391.4-nm excitation and, as in Fig. 11, agrees well with experiment. The lowest dashed curve shows the excitation of the $N_2(C\,^3\Pi_u)$ state predicted by the sum of Eqs. (9) and (18) of II, i.e., the sum of the contributions of secondary and primary electrons. The discrepancy between the results of theory and the excitation coefficients obtained from experiment is about a factor of 250. In spite of the very approxi-
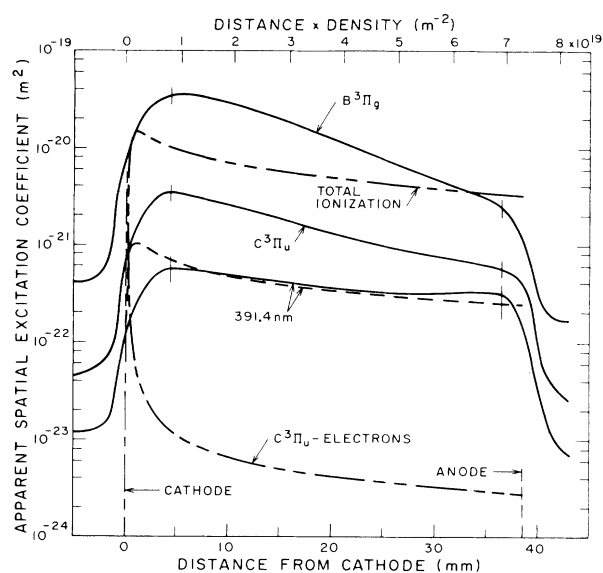

FIG. 12. Comparison of experimental apparent excitation coefficients for $B\,^3\Pi_g$ and $C\,^3\Pi_u$ states and for the 391.4-nm band with theoretical predictions for $E/n = 69$ kTd and an N_2 density of 1.9×10^{21} m^{-3}. The solid curves are drawn through experimental points. The lower dashed curve is the calculated electron excitation coefficient for the $C\,^3\Pi_u$ state, while the middle dashed curve is for the 391.4-nm transition. The uppermost dashed curve is the calculated apparent ionization coefficient and is used in the text for estimating the maximum contribution of excited ions and atoms to the production of $B\,^3\Pi_g$ and $C\,^3\Pi_u$ states. The upper scale shows the product of N_2 density and distance from the cathode. The short vertical lines are as in Fig. 8.

mate nature of the single-beam model for the primary electrons and of the model for the secondary electrons given in II, it seems unlikely that the theory could be in error by such a large factor. Obviously better theories of electron behavior should be considered before ruling out completely direct electron excitation of the $N_2(C\,^3\Pi_u)$ state in the high-E/n experiments. Alternate excitation mechanisms are discussed in Sec. V D.

The situation with regard to the $N_2(B\,^3\Pi_g)$ state is very similar to that for the $N_2(C\,^3\Pi_u)$ state since the sum of the contributions from Eqs. (9) and (18) of II for the $B\,^3\Pi_g$, $W\,^3\Delta$, $B'\,^3\Sigma$, $C\,^3\Pi_u$, and $E\,^3\Sigma_g^+$ states is a factor of 2.4 times that for the $C\,^3\Pi_u$ state, while the apparent excitation coefficient from our experiment is about an order of magnitude larger for the $B\,^3\Pi_g$ state than for the $C\,^3\Pi_u$ state. A potentially important feature of the spatial dependence of the $N_2(B\,^3\Pi_g)$ emission is the rather rapid decrease in intensity with increasing distance from the cathode. Exponential fits to such data yield apparent "attenuation" or "ion avalanche growth" constants which are independent of E/n for $E/n > 10$ kTd.

Empirically we note that at $E/n > 30$ kTd the magnitudes of the 1^+, 2^+, and 1^- signals near the cathode are essentially independent of the E/n while those near the anode change as shown in Fig. 11. The magnitudes 1^+ and 2^+ emission are discussed next.

D. Excitation of N_2 by ions, atoms, and molecules

Figure 1 shows that in principle it is possible for the higher excited states of N_2^+ and of N to transfer excitation to the B and C states of N_2. Since the cross sections for the production of excited ionic states, e.g., N_2^+ $C\,^2\Sigma_u^+$ have essentially the same energy dependence as the total ionization cross section, an upper limit to their contribution is obtained using the single-beam model and replacing $Q_k(v)$ in Eq. (9) of II with the total ionization cross section[15] $Q_i(v)$. The resultant ionization coefficient for $E/n = 69$ kTd is shown by the upper dashed curve of Fig. 12. The cross sections for production of excited ion states with sufficient internal energy to excite the B state of N_2, e.g., vibrationally excited $C\,^2\Sigma_u^+$, are estimated[65] to be less than 10% of the total cross section for ionization. We therefore conclude that the production of B states of N_2 by excitation transfer from thermal-energy-excited ions produced by electron impact is too small to account for the observed N_2 emission. Note that this argument is made even stronger by expected fractional values of the efficiency of excitation transfer, e.g., an upper limit of about 10% for transfer from a state with less than or equal to 100 ns lifetime. There is no N_2^+ state listed[1] with sufficient energy to excite the N_2 $C\,^3\Pi_u$ state by excitation transfer. Note also that the spatial dependence of an excitation process having an electron-energy-dependent cross section similar to that for ionization varies significantly less rapidly with position than the observed N_2 B and C state excitation coefficients.

In view of the very large intensity of the 870- and 820-nm multiplets of lines emitted by N atoms in our experiments, we should consider excitation transfer from these species. An upper limit to the sum of their cross sections is given by the cross section for direct and cascade excitation of the $2p^2 3s\,^4P$ levels, i.e., about 3% of the ionization cross section.[66] Even with a large rate coefficient for excitation transfer of 10^{-15} m³/s, the fraction of the excitation transferred at our N_2 densities of $\sim 2 \times 10^{21}$ m^{-3} is only about 10%. Therefore, excitation transfer from excited N to N_2 cannot account for the observed C- and B-state emission.

Excitation of the $B\,^3\Pi_g$ and $C\,^3\Pi_u$ states by excitation transfer from the singlet states of N_2 is a possibility, although it appears to be unimportant in aurora[56,61] and not to be of major importance in gas discharges.[62,67] At the high electron energies of interest for the data of Fig. 12, the sums of the cross sections[15] for electron excitation of levels with sufficient energy to transfer excitation to the C and B states are 50–70 % of the total ionization cross section. According to Zipf and McLaughlin[68] the $^1\Pi_u$ states of N_2 predissociate with nearly a 100% probability, so that the fraction of the highly excited N_2 able to transfer excitation to the C and B states is significantly less than 1.

Ion-beam experiments[40,41] have demonstrated that collisions of fast N^+ and N_2^+ with N_2 can produce excited N_2^+ with cross sections in the 10^{-22}–10^{-21}-m² range at 100 eV. The cross sections are much larger for the pro-

duction of vibrationally excited N_2 than for N_2^+ ($v = 0$). Excitation of N_2 by ions has been seen in these experiments, but the cross sections appear to be too small to measure. We can estimate the cross sections needed to explain our emission data by noting that (a) the ion current at the cathode[16] is equal to the total current divided by $(1 + \gamma_+)$, (b) the N_2^+ energies are in the 100–200-eV range[58] while N^+ energies are close to free-fall values, (c) the ion velocities at these high E/n are strongly peaked along the direction of acceleration[59] so that from the analog of Eq. (3) for ions the velocity averaged excitation cross section is approximately equal to the apparent excitation coefficient β^k/n. Using this approximation and assuming[69] that γ_+ is about 0.1, the cross section required to explain the 391.4-nm data in Fig. 11 is about 6×10^{-22} m². This value is about an order of magnitude larger than the measured[41] cross section for 391.4-nm excitation by N_2^+ and about 2 orders of magnitude larger than that extrapolated from measurements[40] for N^+. This situation is consistent with the explanation of the 391.4-nm emission in terms of electron excitation in Sec. V C. On the other hand, the cross sections for excitation of vibrationally excited $B\,^2\Sigma_u^+$ molecules by N_2^+ are much larger in this energy range[40,41] and roughly account for the high apparent vibrational temperatures at the higher E/n which were discussed in Sec. III A. Since the beam experiments show that the cross section for $C\,^3\Pi_u$ excitation is small compared to the 391.4-nm cross section, ion excitation of N_2 cannot account for $C\,^3\Pi_u$ data. Unfortunately, the reports of excitation by ion beams are vague regarding the excitation of the $B\,^3\Pi_g$ state. We will assume that this means that the cross sections are small.

The only data we have found on the excitation of N_2 by fast N_2 are those from Sheridan and Peterson[45] on the energy dependence of the cross section for excitation of the $C\,^3\Pi_u$ state. Also they find that the cross section for $C\,^3\Pi_u$ excitation by $N_2(A\,^3\Sigma_g^+)$ metastables is about twice that for excitation by ground state N_2, but do not give any absolute values. Varney,[70] and Haydon and Williams,[43] obtained evidence for fast metastable N_2 in swarm experiments at moderate E/n but did not obtain excitation coefficients. The cross sections for excitation by fast N_2 required to fit the $C\,^3\Pi_u$ and $B\,^3\Pi_g$ data depend on the ratio of fast N_2 to N_2^+, on γ_+ and on the ratio of N_2^+ to N^+ fluxes. Our preliminary models[58] suggest that the ratio of fast N_2 flux to N_2^+ flux is about 5. The models also suggest that the N^+ current is small compared to the N_2^+ current, although this seems contrary to the results of Fletcher and Blevin.[71] We assume $\gamma_+ \sim 0.1$. With these assumptions, the required cross sections for B- and C-state excitation by N_2 of about 100 eV kinetic energy are 20% of the peak excitation coefficients shown in Fig. 12, i.e., 10^{-20} m² for the $B\,^3\Pi_g$ group of states and 10^{-21} m² for the $C\,^3\Pi_u$ state.

Since we find no information on the production of excited N_2 as the result of the bombardment of surfaces of N_2^+ or N^+, all we can do is estimate the yields and excited-state velocities which would be required to fit our emission data at very high E/n. Thus, the applica-

tion of Eq. (8) to an extrapolation of the $B\ ^3\Pi_g$ data of Fig. 12 to the cathode, e.g., $\beta/n = 6 \times 10^{-20}$ m^2, leads to a value of $R_k/(1+\gamma_+)$ of 32, i.e., the impossible requirement of more than 32 excited molecules per incident molecular ion. Because of the shorter radiative lifetime and lower emission, we calculate that the yield of fast excited molecules per incident molecular ion required to explain the extrapolation of the $C\ ^3\Pi_u$ data of Fig. 12 to the cathode is $0.003(1+\gamma_+)$. This yield is about an order of magnitude larger than that found[48] for Hα from H$^+$ at energies of 10 keV. The attenuation distance λ of Eq. (9) calculated using our estimated N$_2{}^+$ drift velocity is only about 1 mm compared to values of about 20 mm required for the data of Fig. 12. Emeleus and Ahmad[50] have suggested that the relatively intense N I spectrum observed near the cathode of the cathode fall in N$_2$ is connected with the dissociative neutralization of molecular ions at the cathode surface. This process does not help in our case since the excited-state species is slower than the reflected ones and since the yield of excited molecules is reduced by the efficiency of excitation transfer. If the incident ions were N$^+$ with a free-fall velocity corresponding to the applied voltage and the reflected excited state had a radiative lifetime of 50 ns, as for the upper levels of the 870- and 820-nm emission, the required values of the yield would be at least 0.06 divided by the efficiency of excitation transfer to the $C\ ^3\Pi_u$ state. This yield seems impossibly large. The attenuation length would be 13 mm, which is about that required. From the preceding considerations it seems unlikely that excited species resulting from fast ions incident on the cathode are important in our N$_2$ experiments.

VI. DISCUSSION

The analyses of experimental emission data for uniform electric field discharges in N$_2$ presented in this paper show that very simple models of electron motion at $E/n > 10$ kTd are capable of explaining the observed excitation of the $v = 0$ levels of the $B\ ^2\Sigma_u^+$ state. The emission from the $v > 0$ levels is quantitatively consistent with excitation by electrons at $E/n < 5$ kTd and semiquantitatively consistent with excitation by ions at $E/n > 20$ kTd. At $E/n < 1$ kTd the 2$^+$ emission from the $C\ ^3\Pi_u$ state varies with position and E/n as expected for electron excitation. At $E/n > 10$ kTd the 2$^+$ emission cannot be explained by any process for which cross sections, etc., are known. Similarly, the spatial dependence of the 1$^+$ emission from the $B\ ^3\Pi_g$ state is consistent with electron excitation for $E/n < 1$ kTd, but is of unknown origin at higher E/n. We suggest that the production of the 1$^+$ and 2$^+$ excitation involves collisions between N$_2$ and fast N$_2$ with cross sections somewhat smaller than the observed apparent excitation coefficients. There are no published cross sections with which to compare these values. The observed excess emission near the cathode at $E/n < 1000$ Td for all N$_2$ bands is unexplained.

The experiments and analyses presented in this paper leave many unanswered questions and suggest a number of future experiments at very high E/n. Firstly, the uncertainties introduced by the indirect procedure for the normalization of the measured relative intensities point to the desirability of absolute intensity measurements using calibrated reference lamps. Secondly, the poorly known quenching rate coefficients, especially for the $B\ ^2\Sigma_u^+$ state at nonthermal energies, should be determined by either time-dependent intensity measurements or by steady-state quenching measurements at fixed E/n and variable n. Thirdly, the time-resolved measurements of the emission at E/n below breakdown should enable one to distinguish between electron-induced excitation and ion- and fast-neutral-induced excitation. Finally, the observation of emission from a field-free region behind a grid cathode may allow separation of ion-induced emission from fast-neutral-induced emission. Attempts to carry out the latter two measurements are currently under way.

In addition to drift-tube experiments, the results point to the need for much more complete cross-section data for ion-molecule collisions at energies up to 10 keV. We have assembled preliminary sets of cross sections from the literature. Particularly important to this work is the absence of data on the excitation of N$_2$ by fast N$_2$ or N. Also it would be very desirable to test the suggestion of Varney[70] and Haydon and Williams[43] on the production of fast N$_2$ metastables in charge-transfer collisions and that of Emeleus and Ahmad[49] on the production of fast excited N in collisions of nitrogen ions with cathode materials.

It is to be hoped that these experiments will encourage future improvements and applications of theory to the calculation of electron and ion transport, excitation and ionization at very high E/n. For example, it is not immediately apparent which nitrogen ions are dominant in N$_2$ at high E/n. The experiments of Fletcher and Blevin[71] show that there is a sudden increase in the ion-induced secondary emission coefficient at E/n near 400 Td. On the basis of ion-mobility measurements this effect is attributed to N$^+$ ions. It is not clear how one reconciles this behavior with the expected dominance of the production of N$_2{}^+$ in electron-impact ionization[72] and with the relatively slow conversion[73] of ground state N$_2{}^+$ to N$^+$ at the ion energies calculated for this E/n.

APPENDIX: BACKSCATTERED ELECTRONS

This appendix summarizes our experimental observations of emission resulting from backscattered electrons

produced when the electrons crossing the discharge strike the anode at very high E/n. Backscattered electrons have been shown by several authors[5,6,11,74] to be a significant source of ionization. We find direct evidence for backscattering by changing the anode material and noting the changes in the spatial dependence of the emission. We have not made spectral scans of emission from the region near the anode, but the large differences in the spatial distribution of emission with the interference filters used in the 337–391-nm range indicate that the emission is not a continuum.[75]

The solid circles of Fig. 13 show apparent excitation coefficients for the $C\,^3\Pi_u$ state from normalized measurements of 337.1-nm emission for $E/n = 12.5$ kTd for a stainless-steel anode and a graphite cathode, while the open circles are for the same conditions except that the electrodes are interchanged. The differences between the data for the stainless steel and graphite anodes at the right-hand side of the figure are attributed to electrons backscattered from the anode. The solid squares for $E/n = 6.3$ kTd in Fig. 7 also show the effects of backscattered electrons on the 337.1-nm emission from positions near the anode. The half widths of the excitation peaks near the anode are difficult to measure because of our limited spatial resolution but correspond to electrons leaving the anode with energies of 30–50 eV, i.e., electrons conventionally called secondaries.[31] See Fig. 6 of II for the maximum range versus distance. With a graphite anode the emission peak is significantly lower than for the stainless-steel anode at 12.5 kTd. At 6.2 kTd the peak near the anode is similar to that of Fig. 13 for stainless steel. This peak is not distinguishable with graphite. At an E/n of 2.5 kTd electron backscattering may be responsible for the difference in the apparent ionization coefficients shown for the stainless-steel and graphite anodes in Fig. 9 although the details are not clear. When interpreting the data of Fig. 13 it must be kept in mind that the data are normalized to the total discharge current and not to the cathode electron current. Also we note that in our model the excitation by electrons versus distance is unchanged by changes in the electrode material. Thus the apparent excitation coefficient curves must be shifted vertically to coincide at say 10 mm from the cathode so as to compare the contributions of backscattered electrons for the various anodes.

The open points of Fig. 13 show that there is a stronger emission of 337.1 nm radiation near the cathode when the cathode is stainless steel than when it is graphite. This effect was also observed at 31 kTd, but with a lower relative amplitude and slope. It was not detected at higher E/n, where the midgap signal varied more rapidly with position. This peak signal near the cathode could be caused by ions reflected from the cathode as excited species, although according to Sec. IV D an excited state yield per ion of greater than 10^{-3} would be required.

The comparison of 391.4 nm data shown in Fig. 13 using stainless steel and graphite electrodes shows that the peaks caused by backscattering extend a large distance from the anode, i.e., they correspond to backscattered

electrons with energies of 600–1000 eV. See Fig. 6 of II. With a graphite anode it was difficult to determine whether backscattering contributed to the 391.4-nm signal or not. We propose that the increase in 391.4-nm emission near $z = 10$ mm for the stainless-steel cathode is due to an increase in the number of electrons leaving the cathode per ion arriving, i.e., an increase in γ_+ for stainless steel relative to graphite. The smaller change in the 337.1-nm emission at $z \sim 10$ mm is consistent with 337.1-nm excitation by fast molecules or ions as proposed in Sec. V provided $\gamma_+ < 1$.

Since no high-resolution spatial data using stainless-steel anodes was obtained at 670 nm and very high E/n, we have no evidence regarding the effects of backscattered electrons on this band.

The smooth curves of Fig. 13 show the emission due to excitation by backscattered electrons as calculated using the single-beam model of electron excitation discussed in Secs. II A, II D, and III D of II. The dashed curve is for the excitation of the 391.4-nm emission, while the solid curve is for the $C\,^3\Pi_u$ state. These curves are calculated for a backscattered secondary energy of 100 eV. The yield of secondary electron production per electron incident on the anode is assumed to be 1.0 as is typical of values for graphite.[32] It probably should be increased significantly for stainless steel and
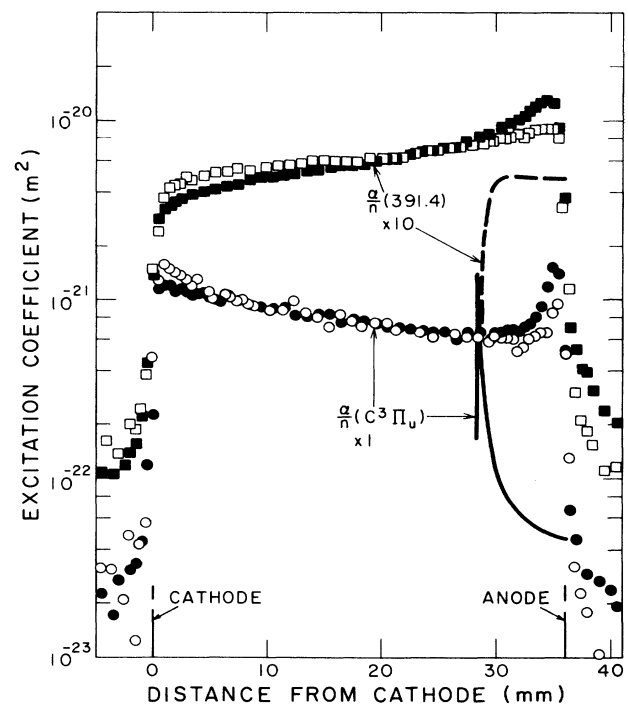

FIG. 13. Spatial dependence of apparent excitation coefficients from N$_2$ discharge showing effect of electrons backscattered from the anode for $E/n = 12.5$ kTd. The smooth curves are calculated for 100-eV electrons leaving the anode. The upper set of points and the dashed curve are for excitation of 391.4-nm emission, while the lower points and solid curve are for the $C\,^3\Pi_u$ state. The solid and open points were obtained using stainless-steel and graphite anodes, respectively.

would be only about 0.1 for 1-keV electrons.[32] In principle, the spatial distributions should be calculated for a wide range of electron energies and then folded into the distributions in energy of backscattered electrons and of "primary" electrons incident on the anode. We have not yet made such calculations and will make only semiquantitative comparisons with experiment. For low energy, i.e., less than 100-eV backscattered electrons, the calculated excitation is spread over distances comparable with the experimental anode peaks and averaging is less important than for higher-energy electrons. We find that for both the $C\,^3\Pi_u$ state and the 391.4-nm band the areas under the calculated curves for 42-eV backscattered electrons are comparable with the experimental anode peaks. Similarly, the area under the calculated 391.4-nm-emission curve for 1000-eV backscattered electrons is comparable with the differences between the measured emission with the stainless-steel and graphite

anodes at positions significantly removed from the anode. On the other hand, when the calculated $C\,^3\Pi_u$ excitation by 1-keV backscattered electrons is spread out over the range of these electrons the average excitation coefficient is small compared to the measured excitation coefficients. This small contribution to the excitation is consistent with the small change in β/n observed for $5 \leq z \leq 25$ mm when the anode material is changed. Obviously, more accurate calculations should be performed in order to improve on these semiquantitative comparisons.

From the comparisons of theory and experiment in Fig. 13 we conclude that the peaks in emission near the anode and the differences in emission with the stainless-steel and graphite anodes are caused by backscattered electrons. The calculated increase in ionization by backscattered electrons is 20–30 % for the conditions of Fig. 13.

*Present and permanent address: Institute of Physics, P.O. Box 75, YU-11001, Belgrade, Yugoslavia.

†Also at Quantum Physics Division, National Bureau of Standards, Boulder, CO 80303, and Physics Department, University of Colorado, Boulder, CO 80309.

[1]A. Lofthus and P. H. Krupenie, J. Phys. Chem. Ref. Data 6, 113 (1977).

[2]A. V. Gurevich, Zh. Eksp. Teor. Phys. 39, 1296 (1960) [Sov. Phys.—JETP 12, 904 (1961)]; Usp. Fiz. Nauk. 120, 319 (1976) [Sov. Phys. Usp. 19, 869 (1976)]; 132, 685 (1980) [23, 862 (1980)].

[3]G. W. Stuart and E. Gerjuoy, Phys. Rev. 119, 892 (1960); E. Gerjuoy and G. W. Stuart, Phys. Fluids 3, 1008 (1960); L. D. Pearlstein and G. W. Stuart, ibid. 4, 1293 (1961).

[4]G. Ecker and K. G. Müller, Z. Naturforsch. 16a, 246 (1961); K. G. Müller, Z. Phys. 169, 432 (1962); K. G. Müller and W. O. Müller, Z. Naturforsch. 30a, 1553 (1975).

[5]K. D. Granzow and G. W. McClure, Phys. Rev. 125, 1792 (1962); K. N. Ul'yanov, Teplofiz Vys. Temp. 16, 1121 (1978) [High Temp. (USSR) 16, 955 (1979)].

[6]A. B. Parker and P. C. Johnson, Proc. R. Soc. London, Ser. A 325, 511 (1971); J. D. Pace and A. B. Parker, J. Phys. D 6, 1525 (1973); D. Bhasavanich and A. B. Parker, Proc. R. Soc. London, Ser. A 358, 385 (1977).

[7]G. Cavalleri and S. L. Paveri-Fontana, Phys. Rev. A 6, 327 (1972).

[8]L. P. Babich and Yu. L. Stankevich, Zh. Tek. Phys. 42, 1669 (1972) [Sov. Phys.—Tech. Phys. 17, 1333 (1973)]; L. P. Babich and Yu. V. Petrov, Fiz. Plasmy 3, 832 (1977) [Sov. J. Plasma Phys. 3, 469 (1977)]; A. P. Dimtriev and L. D. Tsendin, Zh. Eksp. Teor. Fiz. 81, 2032 (1981) [Sov. Phys.—JETP 54, 1071 (1981)]; W. P. Allis, Phys. Rev. 26, 1704 (1982).

[9]L. Friedland, J. Phys. D 7, 2246 (1974); L. Friedland and Yu. M. Kagan, ibid. 15, 1721 (1982); 19, 1019 (1986).

[10]M. Hayashi, in Proceedings of the 4th IEEE Conference on Gas Discharges (Institute of Electrical Engineers, London, 1976), p. 195; K. N. Ul'yanov and V. V. Chulkov, Teplofiz Vyz. Temp. 23, 673 (1985) [High Temp. (USSR) 23, 535 (1986)].

[11]E. J. Lauer, S. S. Yu, and D. M. Cox, Phys. Rev. 23, 2250 (1981); S. S. Yu and R. E. Melendez, Bull. Am. Phys. Soc. 28, 180 (1983).

[12]For a recent discussion of the effects of boundaries on electron transport, see D. R. A. McMahon, Aust. J. Phys. 36, 27 (1983); 36, 45 (1983).

[13]L. C. Pitchford, T. J. Moratz, P. Segur, and M. Yousfi, in Swarm Studies and Inelastic Electron-Molecule Collisions, edited by L. C. Pitchford, V. B. McCoy, A. Chutjain, and S. Trajmar (Springer-Verlag, New York, 1987), p. 115; see also P. Segur, M. Yousfi, and M. C. Bordage, J. Phys. D 17, 2199 (1984).

[14]K.-U. Riemann, Bull. Am. Phys. Soc. 31, 160 (1986).

[15]A. V. Phelps and L. C. Pitchford, Phys. Rev. A 31, 2932 (1985). Note that in this reference the open triangles of Fig. 10 should be solid, while in Fig. 11 the open and solid triangles are interchanged. The cross sections used are tabulated in A. V. Phelps and L. C. Pitchford, Joint Institute for Laboratory Astrophysics (JILA) Information Center Report No. 26, 1985 (unpublished). Note that more recent calculations have shown a noticeable improvement in the agreement between calculated and measured spatial ionization and $C\,^3\Pi_u$ excitation coefficients of Tachibana and Phelps (Ref. 36) when the cross sections for excitation of the $C\,^3\Pi_u$ state in this set are multiplied by 0.67.

[16]M. J. Druyvesteyn and F. M. Penning, Rev. Mod. Phys. 12, 87 (1940).

[17]G. W. McClure and K. D. Granzow, Phys. Rev. 125, 3 (1962); W. P. Allis, G. Fournier, and D. Piqache, J. Phys. (Paris) 38, 915 (1977); A. J. Davies and J. G. Evans, J. Phys. D 13, L161 (1980); P. Segur, M. Yousfi, J. P. Boeuf, E. Marode, A. J. Davies, and J. G. Evans, in Electrical Breakdown and Discharges in Gases, edited by E. E. Kunhardt and L. H. Leusen (Plenum, New York, 1981), p. 331.

[18]Some recent references are V. A. Godyak, Fiz. Plazmy 2, 141 (1976) [Sov. Phys.—Plasma Phys. 2, 78 (1976)]; M. J. Kushner, J. Appl. Phys. 54, 4958 (1983); H. Chatham and A. Gallagher, ibid. 58, 159 (1985).

[19]S. G. Arutunyan, A. V. Ignat'ev, and A. A. Rukhadze, Fiz.

Plazmy **7**, 604 (1981) [Sov. Phys.—Plasma Phys. **7**, 331 (1981)]; J. H. Yee, R. A. Alvarez, D. J. Mayhall, D. P. Byrne, and J. De Groot, Phys. Fluids **29**, 1238 (1986).

[20]D. Turnquist, R. Caristi, S. Freidman, S. Merz, R. Plante, and N. Reinhardt, IEEE Trans. Plasma Sci. **PS-8**, 185 (1980).

[21]G. Yonas and A. J. Toepfer, in *Gaseous Electronics, Gas Discharges,* edited by M. N. Hirsch and H. J. Oskam (Academic, New York, 1978), Vol. 1, pp. 414–421; D. A. Hammer, K. A. Gerber, and A. W. Ali, IEEE Trans. Plasma Sci. **PS-7**, 83 (1979).

[22]A. Buffa, G. Malesani, and G. F. Nalesso, Phys. Rev. A **3**, 955 (1971); L. P. Kubarev, S. A. Uryupin, and L. M. Fisher, Fiz. Plazmy **6**, 187 (1980) [Sov. J. Plasma Phys. **6**, 106 (1980)]; T. Fujiwara, T. Shimada, and K. Sugita, J. Phys. D **16**, 1217 (1983); **18**, 1101 (1985).

[23]P. C. Y. Chen and C. A. Lee, J. Appl. Phys. **42**, 5444 (1971); K. K. Thornber, *ibid.* **52**, 279 (1981).

[24]K. G. Müller and P. Whale, Z. Phys. **179**, 52 (1964).

[25]A. S. Pokrovskaya-Soboleva and B. N. Klyarfel'd, Zh. Eksp. Teor. Fiz. **32**, 993 (1957) [Sov. Phys.—JETP **5**, 812 (1957)], B. N. Klyarfel'd and L. G. Guseva, Zh. Tekh. Fiz. **35**, 306 (1965) [Sov. Phys.—Tech. Phys. **10**, 244 (1965)]; B. N. Klyarfel'd, L. G. Guseva, and A. S. Pokrovskaya-Soboleva, Zh. Tekh. Fiz. **36**, 704 (1966) [Sov. Phys.—Tech. Phys. **11**, 520 (1966)].

[26]G. W. McClure, J. Electron. Control **7**, 439 (1959); G. W. McClure, Phys. Rev. **124**, 969 (1961).

[27]P. Felsenthal, J. Appl. Phys. **37**, 4557 (1966); W. W. Byszewski, M. J. Enright, and J. M. Proud, IEEE Trans. Plasma Sci. **PS-10**, 281 (1982).

[28]G. N. Hays and L. C. Pitchford, Bull. Am. Phys. Soc. **30**, 139 (1985); *ibid.* **31**, 155 (1986).

[29]L. M. Chanin and G. D. Rork, Phys. Rev. **132**, 2547 (1963); M. Hayashi, J. Phys. D **15**, 1411 (1982); J. Fletcher, *ibid.* **18**, 221 (1985); B. W. Aime, J. Fletcher, and M. Sugawara, *ibid.* **18**, 2023 (1985).

[30]A. V. Phelps, B. M. Jelenković, and L. C. Pitchford, *following paper,* Phys. Rev. A **36**, 5327 (1987).

[31]M. J. Schönhuber, IEEE Trans. Power Appar. Syst. **PAS-88**, 100 (1969).

[32]E. J. Sternglass, Phys. Rev. **95**, 345 (1954).

[33]M. I. Datsiev and Yu. I. Belyakov, Zh. Tek, Phys. **39**, 1128 (1969) [Sov. Phys.—Tech. Phys. **14**, 848 (1969)]. See also T. E. Madey and J. T. Yates, Jr., J. Vac. Sci. Technol. **8**, 525 (1971).

[34]G. L. Rogoff, Appl. Opt. **8**, 723 (1969).

[35]B. M. Jelenković and A. V. Phelps, in *Swarm Studies and Inelastic Electron-Molecule Collisions,* edited by L. C. Pitchford, V. B. McCoy, A. Chutjian, and S. Trajmar (Springer-Verlag, New York, 1987), p. 113; in *Proceedings Symposium on Atomic and Surface Physics,* University of Innsbruck, 1986, edited by F. Howorka, W. Lindinger, and T. D. Märk (unpublished), p. 135; Bull. Am. Phys. Soc. **31**, 158 (1986).

[36]K. Tachibana and A. V. Phelps, J. Chem. Phys. **71**, 3544 (1979).

[37]W. R. Pendelton, Jr. and R. R. O'Neil, J. Chem. Phys. **56**, 6260 (1972).

[38]V. V. Urošević, J. V. Božin, and Z. Lj. Petrović, Z. Phys. A **309**, 293 (1983).

[39]V. Degen, J. Quant. Spectrosc. Radiat. Transfer **18**, 113 (1977).

[40]J. H. Moore, Jr., and J. P. Doering, Phys. Rev. **177**, 218 (1969); Ch. Ottinger and J. Simonis, Chem. Phys. **28**, 97

(1978); V. M. Lavrov, M. R. Gochitashvili, V. A. Ankudinov, and B. I. Kikiani, Zh. Tekh. Fiz. **50**, 660 (1979) [Sov. Phys.—Tech. Phys. **25**, 400 (1980)].

[41]S. H. Neff, Astrophys. J. **140**, 348 (1964); J. P. Doering, Phys. Rev. **133**, 348 (1964); C. Liu and H. P. Broida, Phys. Rev. A **2**, 1824 (1970).

[42]S. J. B. Corrigan and A. von Engel, Proc. R. Soc. (London), Ser. A **245**, 355 (1958); H. A. M. Blasberg and F. J. de Hoog, Physica **54**, 468 (1971); A. K. Bhattacharya, Phys. Rev. A **13**, 1219 (1976); J. Appl. Phys. **54**, 3059 (1983).

[43]M. A. Folkhard and S. C. Haydon, J. Phys. B **6**, 214 (1973); S. C. Haydon and O. M. Williams, J. Phys. D **9**, 523 (1976); A. B. Wedding, H. A. Blevin, and J. Fletcher, *ibid.* **18**, 2361 (1985); see also J. Dutton, J. Phys. Chem. Ref. Data **4**, 577 (1975).

[44]The distinction between the spatial excitation and ionization coefficients relevant to the present steady-state experiments and the temporal coefficients is discussed in Ref. 15. The distinction is significant at high E/n in experiments where the energy supplied to electrons produced by ionization is a large fraction of the energy input.

[45]J. R. Sheridan and J. R. Peterson, J. Chem. Phys. **51**, 3574 (1969).

[46]R. C. Flagan and J. P. Appleton, J. Chem. Phys. **56**, 1163 (1972).

[47]R. A. Gottscho and V. M. Donnelly, J. Appl. Phys. **56**, 245 (1984); W. Benesch and E. Li, Opt. Lett. **9**, 338 (1984); A. L. Cappelli, R. A. Gottscho, and T. A. Miller, Plasma Chem. Plasma Proc. **5**, 317 (1985); R. D. May, Appl. Phys. Lett. **46**, 938 (1985).

[48]V. V. Gritsyna, T. S. Kijan, A. G. Koval', and Ja. M. Fogel', Phys. Lett. **27A**, 292 (1968); G. M. McCracken and S. K. Erents, *ibid.* **31A**, 429 (1970); C. Kerkdijk and E. W. Thomas, Physica **63**, 577 (1973); C. Fourrier, G. Lemperiere, and J. M. Poitevin, Phys. Lett. **59A**, 426 (1977).

[49]G. H. Dunn, R. Geballe, and D. Pretzer, Phys. Rev. **128**, 2200 (1962); G. M. McCracken, Rep. Prog. Phys. **38**, 241 (1975).

[50]K. G. Emeleus and N. Ahmad, Nature **201**, 485 (1964); K. G. Emeleus and J. R. M. Coulter, J. Phys. D **16**, 2181 (1983); see also, K. Ohya, K. Isida, and I. Mori, *ibid.* **19**, 157 (1986).

[51]S. A. Lawton and A. V. Phelps, J. Chem. Phys. **69**, 1055 (1978).

[52]W. Legler, Z. Phys. **173**, 169 (1963).

[53]C. G. Freeman and L. F. Phillips, Can. J. Chem. **52**, 426 (1974).

[54]C. H. Chen, M. G. Payne, G. S. Hurst, and J. P. Judish, J. Chem. Phys. **65**, 3863 (1976).

[55]T. W. Carr and S. Dondes, J. Phys. Chem. **81**, 2225 (1977); K. H. Becker, H. Engles, and T. Tatarczyk, Chem. Phys. Lett. **51**, 111 (1977).

[56]H. J. Hartfuss and A. Schmillen, Z. Naturforsch. **23a**, 722 (1968); D. C. Cartwright, J. Geophys. Res. **83**, 517 (1978).

[57]G. I. Sukhinin, G. A. Khramov, and R. G. Sharafutdinov, Zh. Tekh. Fiz. **51**, 1762 (1981) [Sov. Phys.—Tech. Phys. **26**, 1022 (1981)]. Evidence for a smaller charge-transfer cross section for the $B\,^2\Sigma_u^+$ state than for the $X\,^2\Sigma_g^+$ state has been obtained by R. Walkup, R. W. Dreyfus, and Ph. Avouris, Phys. Rev. Lett. **50**, 1846 (1983).

[58]These estimates were made for $N_2{}^+$ drifting through N_2 using a modified form of the model developed for Ar^+ in Ar, in which charge-transfer collisions (see Ref. 60) control the ion motion as described in Ref. 59. The ion-excitation cross sections are from Ref. 40. The Ar model will be published

with the Ar data and analysis.

[59]J. E. Lawler, Phys. Rev. A **32**, 2977 (1985).

[60]R. F. Stebbings, B. R. Turner, and A. C. H. Smith, J. Chem. Phys. **38**, 2277 (1963); M. R. Flannery, P. C. Cosby and T. F. Moran, *ibid*. **59**, 5494 (1973); N. Kobayashi, J. Phys. Soc. Jpn. **38**, 519 (1975).

[61]W. Benesch, J. Chem. Phys. **78**, 2978 (1983). Our measured relative intensities for the $\Delta v = +3$ sequence of the 1^+ system at $n \approx 1.6 \times 10^{21}$ m^{-3} agree well with the high-pressure data in Fig. 2 of this reference.

[62]C. M. Ferreira, M. Touzeau, L. Hochard, and G. Cernogora, J. Phys. B **17**, 4439 (1984).

[63]L. C. Pitchford and A. V. Phelps, Phys. Rev. A **25**, 540 (1982); A. V. Phelps, in *Electrical Breakdown and Discharges in Gas*, Vol. 89a of *NATO Advanced Study Institute, Series B: Physics*, edited by E. E. Kunhardt and L. H. Luessen (Plenum, New York, 1981), p. 109.

[64]We have used the 391.4 excitation cross sections of W. L. Borst and E. C. Zipf, Phys. Rev. A **1**, 834 (1970). See also J. W. McConkey and I. D. Latimer, Proc. Phys. Soc. London. **86**, 463 (1965); H. Nishimura, J. Phys. Soc. Jpn. **24**, 130 (1968); J. F. M. Aarts, F. J. De Heer, and D. A. Vroom, Physica **40**, 197 (1968); B. N. Srivastava and I. M. Mirza, Phys. Rev. **176**, 137 (1968); P. N. Stanton and R. M. St. John, J. Opt. Soc. Am. **59**, 252 (1969).

[65]C. H. Jackman, R. H. Garvey, and A. E. S. Green, J. Geophys. Res. **82**, 5081 (1977).

[66]J. F. M. Aarts and F. J. De Heer, Physica **52**, 45 (1971); M. J. Mumma and E. C. Zipf, J. Chem. Phys. **55**, 5582 (1971). Cross sections for electron excitation of the 820-nm line are given by W. F. Sheridan, O. Oldenberg, and N. P. Carleton, in *Proceedings of the 2nd International Conference on the Physics of Electronic and Atomic Collisions*, edited by B. Bederson (Benjamin, New York, 1961), p. 159.

[67]O. V. Ravodina and T. N. Popova, Opt. Spektrosk. **40**, 652 (1976) [Opt. Spectrosc. **40**, 372 (1976)].

[68]E. C. Zipf and R. W. McLaughlin, Planet. Space Sci. **26**, 449 (1978).

[69]P. Mahadevan, G. D. Magnuson, J. K. Layton, and C. E. Carlston, Phys. Rev. **140**, A1407 (1965); D. W. Vance, *ibid*. **169**, 263 (1968).

[70]R. N. Varney, Phys. Rev. **157**, 113 (1967); **157**, 116 (1967); **175**, 98 (1968).

[71]J. Fletcher and H. A. Blevin, J. Phys. D **14**, 27 (1981); see also A. V. Bondarenko, Zh. Tech. Phys. **43**, 821 (1973) [Sov. Phys.—Tech. Phys. **18**, 515 (1973)].

[72]T. D. Märk, in *Electron Impact Ionization*, edited by T. D. Märk and G. H. Dunn (Springer-Verlag, New York, 1985), Fig. 5-32.

[73]W. B. Maier, J. Chem. Phys. **55**, 2699 (1971).

[74]B. N. Klarfel'd, L. G. Guseva, and V. V. Vlasov, Zh. Tek, Phys. **38**, 1288 (1968) [Sov. Phys.—Tech. Phys. **13**, 1056 (1969)].

[75]Studies of the continuum emission resulting from ion bombardment of surfaces are reviewed by G. E. Thomas, Surf. Sci. **90**, 381 (1979).